Astron. Astrophys. 274, 478–486 (1993)

ASTRONOMY AND ASTROPHYSICS

Surface waves as the origin of the Evershed phenomenon

M. Bünte, G. Darconza, and S.K. Solanki

Institute of Astronomy, ETH Zentrum, CH–8092 Zürich, Switzerland

Received December 9, 1992; accepted March 13, 1993

Abstract. We investigate the spectral signature of magnetoacoustic-gravity surface waves (MAGS-waves), which we expect to exist at the interface between the lower boundary of the magnetic field of the sunspot penumbra and the non-magnetic gas below. MAGS-waves have a number of properties that make them attractive candidates for explaining the photospheric Evershed effect: 1. Since they transport only energy but no mass, they resolve the problem of mass conservation at the outer penumbral boundary. 2. Since they are restricted to magnetic interfaces, they are only (or dominantly) present in the penumbra and absent in the umbra. 3. The phase relation between the temperature, the horizontal, and vertical velocity perturbations leads to line shifts and asymmetries in observations at the limb, but none at disc centre. 4. The amplitude of the velocity perturbation drops approximately exponentially with height, in good agreement with observations. 5. Waves travelling in opposite directions with respect to the observer produce oppositely directed line shifts and asymmetries, making it straightforward to explain the opposite shifts and asymmetries observed in the limb-side and centre-side penumbra.

Key words: Sun: magnetic fields – sunspots – line: profiles – MHD

1. Introduction

Evershed (1909) discovered that Fraunhofer lines in spectra of sunspot penumbrae are displaced. In the limbward penumbra the line profiles are red-shifted, whereas in the centreward penumbra the profiles are blue-shifted. This effect is more pronounced for spots observed closer to the limb. Apart from the often rather small displacement of the line core, the line profiles show a pronounced asymmetry (e.g. Schröter 1965; Stellmacher & Wiehr 1980; Schröter et al. 1989). Evershed himself suggested that the line-shifts could be explained by matter flowing out of the penumbra, and his suggestion has been widely accepted.

Meyer & Schmidt (1968) showed that such a flow will occur along an arched magnetic flux tube connecting two footpoints (of equal gravitational potential) on the solar surface whenever the gas pressures at the two footpoints differ. The flow accelerates away from the high pressure footpoint in the penumbra to the low pressure footpoint, a pore, knot or magnetic element in the surroundings of the spot. This so-called siphon flow model, however, is in serious conflict with mass conservation. If the Doppler shifts are indeed interpreted as mass flows, the observed mass flux from the deeper layers of the penumbra is much larger than that observed in the superpenumbral magnetic canopy (Solanki et al. 1992, 1993). Furthermore, no motions can be detected at any photospheric height in the structures forming the outer footpoints of the magnetic arches which emanate from the penumbra (e.g. Stenflo & Harvey 1985; Solanki 1986).

A completely different approach to the problem was taken by Maltby & Eriksen (1967), who suggested that the Evershed effect might be due to progressive, acoustic waves travelling parallel to the solar surface, radially outwards from the umbra. They showed that these waves may produce net line asymmetries due to a correlation between temperature and velocity. Since waves do not transport matter, the missing mass-flux problem is automatically solved. On the other hand, this wave model faces a new problem: acoustic waves do not have a preferred direction of propagation. Hence the acoustic wave model cannot explain why the Evershed effect is only seen towards the limb but not at disc centre (e.g. Maltby 1964).

The difficulties associated with the interpretation of the Evershed effect as an acoustic wave phenomenon are not greater than those involved in the siphon flow model. Whereas the latter provides a natural explanation of the directional character of the Evershed phenomenon, the former offers an elegant solution to the missing mass-flux problem. In this paper we consider a model which combines these two aspects. It is based on surface waves, i.e. waves that propagate along the interface between two media and decay perpendicularly away from it. Such waves are likely to exist at the boundary between the penumbral magnetic field and the underlying non-magnetic convection zone. For large horizontal wavelengths they might appear as running penumbral waves as suggested by Nye & Thomas (1976b). Their properties stem from the combined influence of gravitational, compressional, and magnetic restoring forces, suggesting the term magneto-acoustic gravity surface (MAGS-) waves (Miles & Roberts 1992; Miles et al. 1992). Since temperature and horizontal velocity perturbations are correlated in these waves, they

Send offprint requests to: M. Bünte

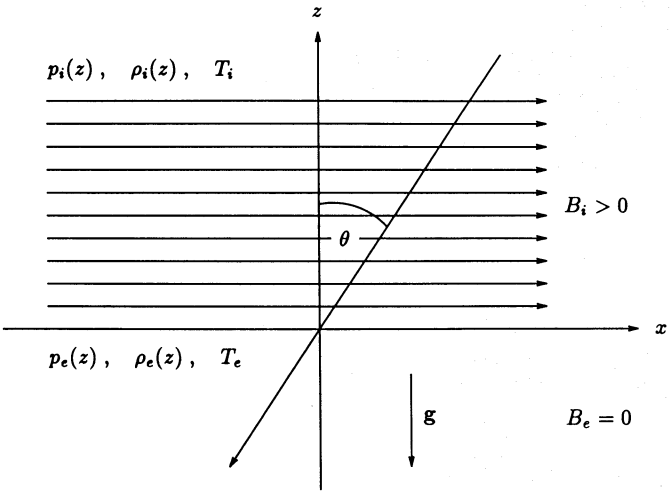

Fig. 1. The stratified two layer equilibrium model with interface at $z = 0$. Quantities with subscript 'i' refer to the (internal) upper magnetic region, those with subscript 'e' to the (external) lower non-magnetic region. We observe the interface along a line-of-sight, at an angle θ to the vertical

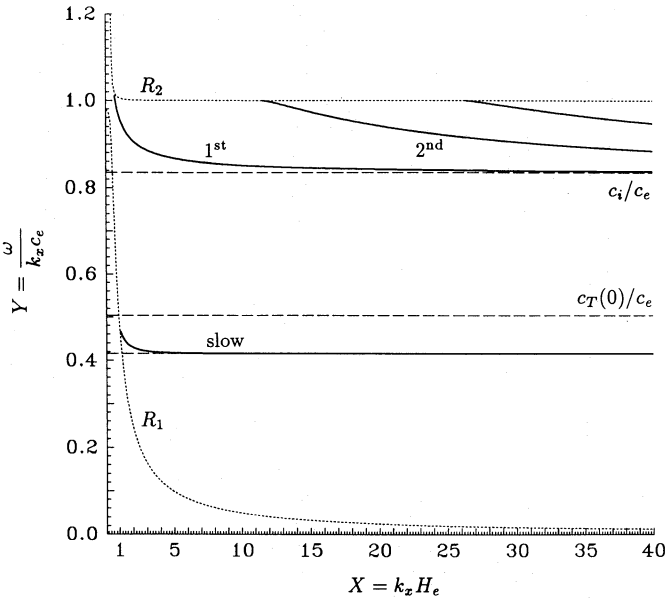

Fig. 2. Dispersion diagram of magneto-acoustic gravity surface modes. Nondimensional phase speed Y vs. non-dimensional horizontal wavenumber X for $c_i/c_e = 0.835$ and $v_A(0)/c_e = 0.632$. For a given wavenumber X surface modes are restricted to phase speeds Y between the two cutoff frequencies $R_1(X)$ and $R_2(X)$ (dotted curves) given by Eq. (3). Within this region, there is a separation into slow ($Y < c_T(0)/c_e$) and fast ($Y > c_i/c_e$) modes. The lower horizontal dashed line is the asymptote to which the slow mode develops in the case of zero gravity (see Miles et al. 1992)

are expected to affect line profiles when observed away from disc centre (Darconza 1992). This property of MAGS-waves is the topic of our investigation.

Bearing in mind that our model is very rudimentary, we have not attempted to quantitatively reproduce the observations, restricting ourselves to qualitative comparisons. The present paper is therefore exploratory in nature. In Sect. 2 we briefly describe the various surface modes and their eigenfunctions. Section 3 contains a description of our simple penumbral model and its analysis in radiative transfer calculations. The results are presented in Sect. 4, and our conclusions are discussed in Sect. 5, followed by suggestions for improving the model. The most important formulae describing magneto-acoustic gravity waves in general and the surface wave solutions for our two layer model in particular are given in appendices A & B.

2. Magneto-acoustic gravity waves

We consider surface waves at a horizontal current sheet in the photosphere separating an upper magnetic from a lower non-magnetic region as shown in Fig. 1. This two-layer model with a sharp interface, where the magnetic field changes discontinuously, may serve as a first approximation to the field structure of the penumbra of a large sunspot. The basic equations for magneto-hydrodynamic (MHD) wave propagation in an ideal, perfectly conducting, compressible, and stratified plasma are the equations describing the continuity of mass, momentum and energy, together with the induction equation and an equation of state. Effects of viscosity are neglected, and the perturbations are assumed to be adiabatic. The formal solution of the problem has been given by Miles et al. (1992; see also Nye & Thomas 1976a) so that we restrict our discussion to some general statements.

2.1. Solution of the linearized equations

We study linear perturbations (index '1') of the equilibrium configuration (index '0') shown in Fig. 1. Linearization of the basic MHD equations allows us to reduce the problem to one ordinary differential equation in the vertical velocity perturbation, v_{1z}. We seek solutions for the perturbations whose dependence on time t and horizontal coordinate x is given by

$$\exp[i(\omega t - k_x x)] \,, \tag{1}$$

where ω is the frequency and k_x the horizontal wave-number. The resulting equation governing the vertical velocity amplitude (indicated by a circumflex) $\hat{v}_{1z}(z)$ is given in appendix A, Eq. (A1), along with the expressions for all the other perturbations in terms of $\hat{v}_{1z}(z)$ and its first derivative, Eqs. (A2).

Since for all surface waves $\mathrm{d}v_{1z}/\mathrm{d}z$ is in phase with v_{1z}, it follows from these expressions that, except for B_{1z}, all perturbations are phase-shifted equally by $\pi/2$ with respect to v_{1z}. Consequently, the perturbations in horizontal velocity and temperature are correlated and lead to a net line shift in observations close to the limb. In contrast, due to the phase lag between v_{1z} and T_1, there is no asymmetric influence on the line profile for observations at disc centre. This is in good qualitative agreement with observations.

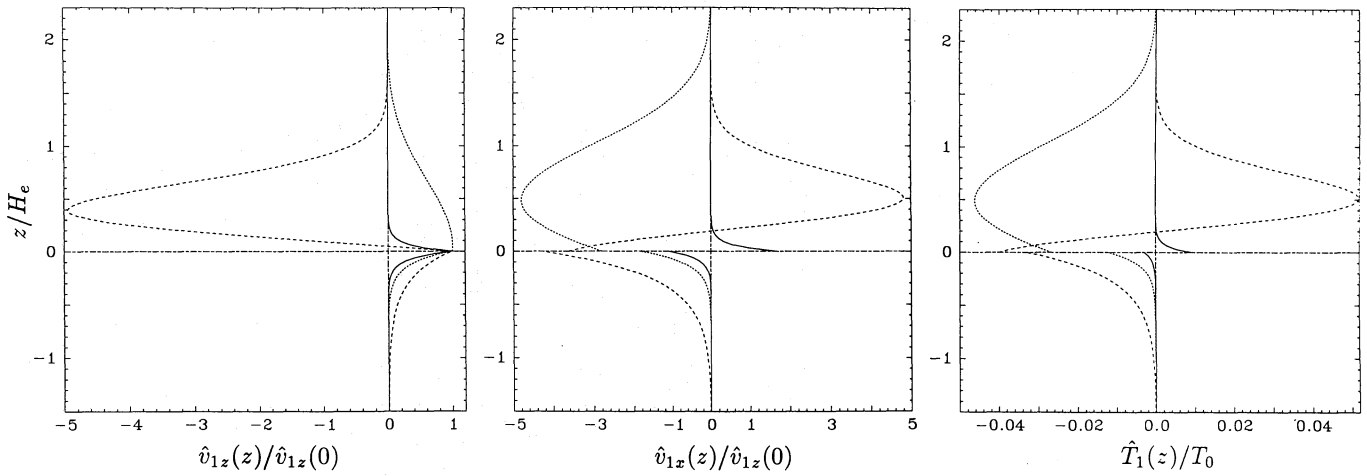

Fig. 3. The eigenfunctions of the vertical velocity (left), the horizontal velocity (middle), and the temperature perturbations (right) arising from the slow mode (solid), the 1st (dotted), and the 2nd (dashed) harmonic mode, respectively, vs. height z/H_e, where H_e = 150 km is the external pressure scale height. The modes have been calculated for the model atmosphere described in Sect. 3.1 with c_i/c_e = 0.835 and $v_A(0)/c_e$ = 0.632. The horizontal wavelength of the modes is λ_x = 63.4 km (X = 15 in Fig. 2), the periods P are 18.4 s, 9.0 s, and 7.8 s, respectively. The magnitude of the relative temperature perturbation depends upon the absolute velocity amplitude $\hat{v}_{1z}(0)$ which in this case was chosen 100 m/s. The equilibrium temperature T_0 is given by T_e = 6420 K for $z < 0$ and by T_i = 4530 for $z > 0$

2.2. The two-layer equilibrium

Our crude penumbral model consists of two isothermal layers (with temperatures $T_{i,e}$ = constant) the upper one of which is permeated by a constant horizontal magnetic field (B_i = constant, B_e = 0). The equilibrium therefore is one of hydrostatic balance throughout the entire model with a density stratification according to $\rho_{i,e}(z) = \rho_{i,e}\exp(-z/H_{i,e})$, where $\rho_{i,e}$ are the densities above ($z > 0$) and below ($z < 0$) the interface, $H_i = c_i^2/(\gamma g)$ and $H_e = c_e^2/(\gamma g)$ the constant scale-heights, c_i and c_e the respective isothermal sound speeds, γ the adiabatic exponent, and g the gravitational acceleration. For this equilibrium the problem can be solved analytically. The solution for $\hat{v}_{1z}(z)$ is given in appendix B, Eq. (B1). Note that in this case the Alfvén speed, $v_A(z) = B_i/\sqrt{4\pi\rho_i(z)}$, increases with height as $\exp[z/(2H_i)]$, leading to the appearance of harmonics of the basic modes of the system.

2.3. The dispersion relation

The dispersion relation of the above equilibrium configuration follows from the pressure balance at the interface and is given in Eq. (B3). Due to its transcendental character it must be studied numerically. For this purpose it is convenient to choose a non-dimensional notation, introducing the quantities

$$X = k_x H_e\ , \qquad Y = \frac{\omega}{k_x c_e}\ , \tag{2}$$

where X is the non-dimensional wave number and Y the phase speed of the waves along the interface in units of the external sound speed. All the other quantities appearing in the dispersion relation can be expressed in terms of c_i/c_e, $v_A(0)/c_e$, γ, X, and Y. For all our calculations we have used $\gamma = 5/3$.

2.4. Surface modes

The solution in the non-magnetic domain may decay or oscillate in the z-direction depending on frequency and given wavenumber k_x. Non-oscillatory (i.e. surface) modes are restricted to a particular region in the ω-k_x-diagram (X-Y-plane) whose boundaries $R_1(X)$ and $R_2(X)$ are given by

$$R^2_{1,2}(X) = \frac{1}{8X^2}\left\{1 + 4X^2 \mp \sqrt{\left(1+4X^2\right)^2 - 64\frac{\gamma-1}{\gamma^2}X^2}\right\}\ . \tag{3}$$

The surface modes exist in the range $R_1 < Y < R_2$, as shown in Fig. 2. In the region above the upper dotted curve, $R_2(X)$, any perturbation of the interface decays due to the downward emission of gravitationally modified acoustic waves. In the region below the lower dotted curve, $R_1(X)$, the damping is due to the emission of gravity waves instead.

In the absence of gravity, a magnetic interface supports two surface waves: a slow magneto-acoustic mode, indicated by the lowest horizontal dashed line in Fig. 2, and also a high-phase-speed or fast magneto-acoustic mode if the field free region is warmer than the magnetic region (i.e. $c_i < c_e$) and $v_A(0) > c_i$ (Roberts 1981; Miles & Roberts 1989). In the stratified case, the Alfvén speed increases exponentially with height, leading to the appearance of additional trapped harmonic modes in the high phase speed domain (Nye & Thomas 1976a,b; Miles et al. 1992). They correspond to magnetically modified p-modes and exist even if $v_A(0) < c_i$, i.e. in the case of a weak magnetic field. As the magnetic field strength is increased, the 1st harmonic (corresponding to a magnetically modified f-mode) develops into the fast mode and the higher harmonics are restricted to ever larger values of X, i.e. shorter horizontal wavelengths. Figure 2 shows the modes obtained for c_i/c_e = 0.835 and $v_A(0)/c_e$ = 0.632,

the values which we have used throughout our calculations (see Sect. 3). Note that the boundaries of the surface mode domain, R_1 and R_2, set an upper limit to the period and wavelength of each surface mode (except for the 1st harmonic which reappears close to $X = 0$, i.e. at very large horizontal wavelengths). For our model described in Sect. 3.1 the maximum wavelengths for the slow mode, the 1st, and the 2nd harmonic are 950, 1570, and 80 km, respectively, corresponding to 1.2″, 2.2″, and 0.1″ on the solar disc at vertical incidence. Although it is possible to resolve the slow mode and the 1st harmonic close to the cutoff at high spatial resolution, almost all the wavelengths lie considerably below the currently achievable spatial resolution limit.

2.5. Remarks on surface mode eigenfunctions

The characteristic feature of surface waves is that they propagate only parallel to the interface and decay in the perpendicular direction away from it. In the unstratified case this decay is strictly exponential and more rapid in the magnetic layer (Miles & Roberts 1989; Jain & Roberts 1991). In the presence of gravity, however, the perturbations arising from the harmonic modes not only penetrate much farther into the magnetic region, but may even assume their maximum there, i.e. at a certain vertical distance *above* the interface at $z = 0$ (cf. Fig. 3). This is a fundamental difference between the low and high phase speed modes of the system and of great importance for their spectral signature discussed in the subsequent sections. As an example, Fig. 3 shows the eigenfunctions of the velocity and temperature perturbations arising from the slow mode and the 1st and 2nd harmonics with wavelengths $\lambda_x = 63.4$ km ($X = 15$ in Fig. 2) as a function of z/H_e for the model atmosphere described in Sect. 3.1 with $c_i/c_e = 0.835$ and $v_A(0)/c_e = 0.632$. For larger values of X (i.e. smaller horizontal wavelength λ_x), we obtain qualitatively similar results.

Note also the magnitude of $\hat{v}_{1x}$ relative to $\hat{v}_{1z}$: the largest velocity fluctuations occur in the horizontal direction. The maximum and minimum values of $\hat{v}_{1x}(z)/\hat{v}_{1z}(0)$ and of $\hat{T}_1(z)/T_i$ for $z > 0$ and $\hat{T}_1(z)/T_e$ for $z < 0$ vary differently with wavelength for the various modes. Whereas they increase with increasing wavelength for the slow mode, the opposite is the case for the 1st harmonic. The perturbation amplitudes of the 1st harmonic grow dramatically for $\lambda_x < 100$ km. This indicates that the linear treatment looses its validity for very short wavelengths, even for small $\hat{v}_{1z}(0)$.

3. Model construction and spectroscopic analysis

3.1. Perturbation of the equilibrium model

In this section we describe the main features and properties of our model. The equilibrium consists of two layers, an upper magnetic and a lower non-magnetic atmosphere. For the latter we use the convection zone model of Spruit (1977), for the former the penumbral model of Ding & Fang (1989) on which we superimpose a constant horizontal magnetic field B_i. The

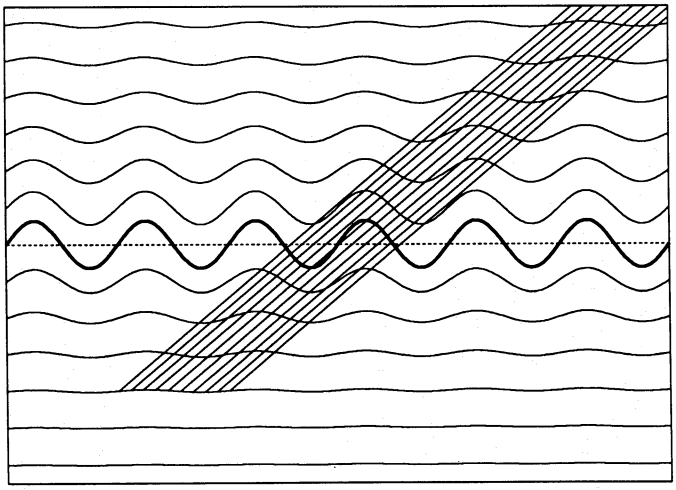

Fig. 4. Schematic diagram showing the bundle of parallel rays along which we observe MAGS-waves (solid wavy lines) propagating along the interface (dashed horizontal line) between the upper magnetic and the lower non-magnetic layer. The rays enter the model at an angle θ to the vertical (corresponding to $\mu = \cos\theta$ on the solar disc) and are uniformly distributed over a full wavelength

two atmospheres are matched at a prescribed height $z = z_0$ by requiring pressure balance

$$p_i(z_0) + \frac{B_i^2}{8\pi} = p_e(z_0) \; . \tag{4}$$

In order to properly resolve the interface at $z = z_0$ we recalculate the τ_c-scale at 5000 Å with a prescribed upper limit of 0.1 for the $\log \tau_c$-stepsize.

After having constructed the equilibrium model, we determine in a second step the perturbations arising in both half-spaces from the surface waves at the interface $z = z_0$. For this purpose we use the atmospheric parameters at the interface as the input values for the isothermal wave model described in the previous section. This fixes the values of the basic non-dimensional parameters c_i/c_e and $v_A(0)/c_e$. Taking $\gamma = 5/3$, the dispersion relation, Eq. (B3), is then solved for a given horizontal wavenumber, k_x, under the constraints described in Sect. 2.4. This yields the allowed frequencies $\omega(k_x)$ for the various modes of the system and hence the respective eigenfunctions $\hat{v}_{1z}(z)$ from Eq. (B1). The perturbations in the other atmospheric parameters follow from Eqs. (A2).

Note that whereas the equilibrium model in Sect. 2 consists of two isothermal layers, the equilibrium part of the model underlying the radiative transfer is composed of two semi-empirical non-isothermal atmospheres. In photospheric levels where temperature gradients are large, this procedure is questionable, and it is likely that the vertical temperature variation will affect mode structure and eigenfunctions of the surface waves. The computation of the "real" surface modes, however, is a formidable task by itself and beyond the scope of this paper. To obtain a first rough estimate of the spectral signature of surface waves we have therefore used the available theory for two isothermal layers (Miles et al. 1992).

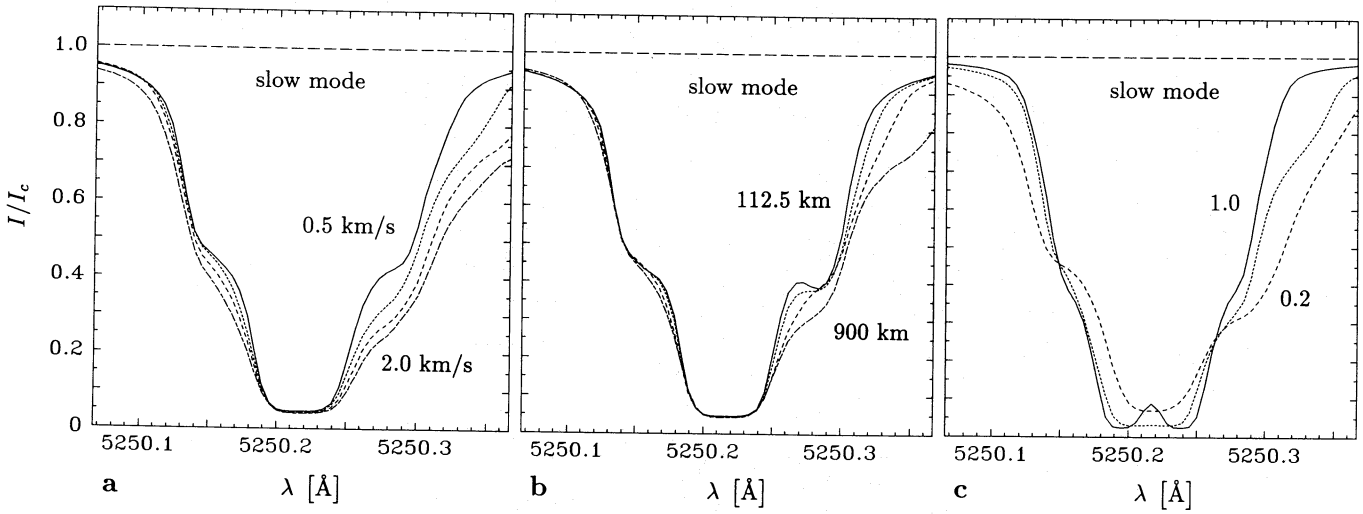

Fig. 5. Line profiles of the Fe I 5250.2 Å line calculated in the presence of the slow mode. **a**: $\mu = 0.34$, $\lambda_x = 700$ km, $\hat{v}_{1z}(0)$ in km/s: 0.5 (solid), 1.0 (dotted), 1.5 (dashed), and 2.0 (dot-dashed). **b**: $\mu = 0.34$, $\hat{v}_{1z} = 1$ km/s, λ_x in km: 112.5 (solid), 225 (dotted), 450 (dashed), and 900 (dot-dashed). **c**: $\lambda_x = 700$ km, $\hat{v}_{1z}(0) = 1$ km/s, $\mu = \cos\theta$: 1.0 (solid), 0.6 (dotted), and 0.2 (dashed)

For a given choice of the two atmospheres we are free to prescribe the vertical position of the interface, z_0, the unperturbed magnetic field strength, B_i, and the wavelength of the surface wave, λ_x. Furthermore, we must prescribe the amplitude $\hat{v}_{1z}(0) = \hat{v}_{1z}(z_0)$ of the vertical velocity perturbation at the interface and finally, if more than one frequency is compatible with the given parameters, we must choose one of the allowed modes. In all the calculations presented here the interface resides at $\tau_c = 1$ of the unperturbed lower atmosphere. For the above mentioned choice of atmospheric models this gives $p_e = 1.274 \cdot 10^5$ dyn/cm^2, $\rho_e = 3.07 \cdot 10^{-7}$ g/cm^3, $T_e = 6420$ K, and $p_i = 0.655\,p_e$, $\rho_i = 0.938\,\rho_e$, $T_i = 0.706\,T_e$ for a magnetic field strength $B_i = 1000$ G, yielding $c_i/c_e = 0.835$ and $v_A(0)/c_e = 0.632$. The upper magnetic atmosphere is cooler than the underlying non-magnetic convection zone, giving rise to the propagation of harmonic modes along the interface (in addition to the slow magneto-acoustic gravity mode).

3.2. Radiative transfer

To study the effect of MAGS-waves on the profiles of spectral lines at various positions on the solar disc we "observe" the model structure along a number of parallel rays entering the atmosphere at an angle θ to the vertical. At a fixed time t_0 the rays are distributed equidistantly over one horizontal wavelength of the wave, as shown in Fig. 4. In a first step, we determine the atmospheric structure including the perturbations arising from surface mode propagation. In a second step, we recalculate the τ_c-scale (using the code by Gustafsson 1973) and the atmospheric parameters along each ray. For the velocity field, $\boldsymbol{v}_1$, we determine the projection onto the line of sight (positive velocity being directed away from the observer). In a final step we compute the average of the line profiles emerging along the various rays (1.5-D radiative transport). For details on the physics underlying the radiative transfer calculations we refer to Solanki (1987). Averaging over a full wavelength of the wave is equivalent to considering one single ray at different times covering a full wave period. The importance of this procedure lies in the fact that only net shifts and asymmetries can be identified with the Evershed effect, since the observed signal resembles a steady flow. If the wavelength lies below the spatial resolution, then the net shift can be seen while the oscillation remains invisible.

4. Results

We investigate the effect of MAGS-waves on the line profile of the well-studied neutral iron line at 5250.2 Å. First we describe the basic influence of surface waves on the line profiles and discuss the influence of prescribed amplitudes and wavelengths (Figs. 5a & b). Then we demonstrate that the influence of surface waves vanishes at disc centre and is observable only towards the limb (Fig. 5c). Finally, we discuss differences in the spectroscopic signature of the various surface modes (slow mode, first, and higher harmonics; Figs. 5a & 6).

4.1. Line asymmetries of Fe I 5250.2Å

Figure 5a shows line profiles calculated at $\theta = 70°$ in the presence of the slow mode with $\lambda_x = 700$ km and different values of the vertical velocity amplitude $\hat{v}_{1z}(0)$. The resulting line profiles show only a small shift in the line core and strong asymmetries in the wings, which become more prominent as the amplitude of the perturbations is increased. This behaviour is a direct consequence of the exponential decay of slow-mode perturbations with height (Fig. 3). The line wings are formed deeper in the atmosphere, where the perturbations due to the waves are large, while the line core is formed higher up where the perturbations are small. Consequently, for a spectral line formed higher in the atmosphere the net effect will be smaller, in agreement with the observed drop in Evershed velocity with height.

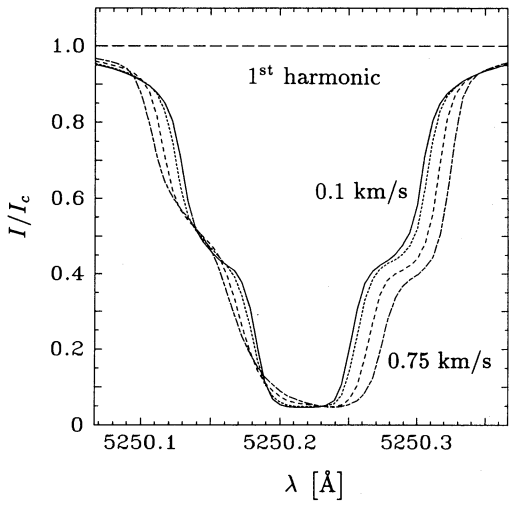

Fig. 6. Line profiles calculated at $\mu = 0.34$ ($\theta = 70°$) in the presence of the 1st harmonic with $\lambda_x = 700$ km. Different profiles correspond to different vertical velocity amplitudes $\hat{v}_{1z}(0)$ in km/s: 0.1 (solid), 0.25 (dotted), 0.5 (dashed), and 0.75 (dot-dashed)

As shown in Fig. 5b the line asymmetry also increases if for fixed amplitude $\hat{v}_{1z}(0)$ the wavelength λ_x is increased. This is due to the increasing horizontal velocity and temperature perturbations of the slow mode with increasing wavelength (cf. Sect. 2.5). The profiles shown in Figs. 5 & 6 have been calculated for waves propagating towards the observer. Note that due to the phase relations between horizontal velocity and temperature perturbations (and the specific temperature dependence of the Fe I line) this results in a redshift of line core and wings. For waves propagating away from the observer, we obtain a blueshift. The depth of the line profiles in Figs. 5 and 6 is larger than observed in the penumbra. The excess line depth is entirely due to the chosen temperature stratification of the unperturbed model atmosphere, in particular the large temperature jump just above $\tau_c = 1$, and is not related to the wave perturbations.

4.2. The centre-to-limb variation of the MAGS-wave signature

In Fig. 5c we have plotted three profiles of Fe I 5250.2 Å computed in the presence of the slow mode with $\lambda_x = 700$ km at three different positions on the solar disc: $\mu = 1.0$ ($\theta = 0°$; solid), $\mu = 0.6$ ($\theta = 53°$; dotted), and $\mu = 0.2$ ($\theta = 78.5°$; dashed). Note that whereas the profile at disc centre is completely symmetric and unshifted, the two other profiles show an increasing asymmetry and line core shift towards the limb. In addition, both the half width and the equivalent width of the line increase towards the limb.

This change in line shape and equivalent width is determined by a number of parameters. As pointed out in Sect. 2.1 the perturbations in temperature are in phase with the horizontal velocity, but completely uncorrelated with the vertical velocity component. Hence, the line-of-sight velocity for observations at disc centre shows no correlation with the temperature perturbations and therefore leaves the emerging line profile unchanged, except for some broadening. Towards the limb the line profile is increasingly affected by the horizontal velocity and the correlated temperature perturbations, which gives rise to asymmetric line profiles. Note also that, due to $\hat{v}_{1x}/\hat{v}_{1z} > 1$ (Fig. 3, Sect. 2.5), the profiles formed near the limb are broader than the profile formed at disc centre. To first order the line broadening depends solely on the amplitude of the line-of-sight velocity component and not on any phase correlation. Note, however, that the increase in the equivalent width requires an additional ingredient, namely the presence of strong gradients in the line-of-sight velocity and temperature near the limb, which are absent at $\mu = 1$. They arise only along an inclined line-of-sight since it samples different phases of the wave-perturbations at different heights. The effect is expected to increase with decreasing λ_x. Note that near the limb the line depth decreases due to the fact that $\tau_c = 1$ is reached at a higher level in the atmosphere.

4.3. Slow and fast modes

The different modes have quite different influences on the line profiles. Comparison of Figs. 5a and 6 shows that whereas the slow mode mainly introduces strong asymmetries in the line wings, while leaving the line core unchanged, the 1st harmonic appears to broaden and shift the line profile by approximately the same amount at all intensity levels. The net effect is that the line as a whole remains relatively symmetric, but is shifted.

The reason for this different behaviour lies in the structure of the eigenfunctions for the given set of parameters. Whereas the slow mode decays monotonically with height, the horizontal velocity and temperature amplitudes of the 1st harmonic increase within the first pressure scale height above the interface and start to decline only farther up (cf. Fig. 3). This large vertical range of the perturbations is a common feature of all high phase speed modes. Hence these modes have a considerable influence also on the line core, which is formed at higher levels in the atmosphere. Furthermore, they should produce asymmetries even if the interface lies deeper in the atmosphere, in which case the slow mode only minutely influences the line wings. This expectation is confirmed by calculations.

The various modes also differ in the magnitude of the perturbations relative to the equilibrium values (cf. Fig. 3). The perturbations are usually larger for the high phase speed modes such that, e.g., the 2nd harmonic strongly influences both the wings and the core of the line, even for small $\hat{v}_{1z}(0)$. Decreasing the horizontal wavelength reveals further differences between the modes. For certain modes (e.g. the slow mode and the 2nd harmonic) the magnitudes of the perturbations decrease, while for others (e.g. the 1st harmonic) they increase.

5. Discussion and conclusions

We have explored the spectral signature of MAGS-waves propagating along the horizontal interface between an upper magnetic and a lower non-magnetic stratified atmosphere. We interpret

this magnetic configuration as a very simple model of the expanding penumbra of a sunspot overlying the quiet convection zone. It lies in the nature of a linear wave theory that the amplitudes of the wave perturbations are small compared to the equilibrium values. In spite of their smallness they can greatly influence spectral lines. We find that surface waves can produce small shifts in the line core of Fe I 5250.2 Å and large shifts in its wings when observed towards the limb. This signature is in qualitative agreement with the Evershed effect observed in sunspot penumbrae.

As mentioned in the introduction and discussed in detail by Solanki et al. (1993), mass conservation is a severe problem at the outer penumbral boundary if the Evershed effect is interpreted as a steady mass flow (e.g. as a siphon flow). Our attempt to explain the Evershed effect as a surface wave phenomenon has the advantage that mass conservation is a priori satisfied. A wave model has already been suggested by Maltby & Eriksen (1967), but the acoustic waves they consider have no directional character and should propagate in basically all directions. Hence, in their model the centre-to-limb variation of the line shifts and asymmetries is hard to explain. Surface waves, on the other hand, propagate only along the surface they live on. Furthermore, their perturbations in temperature are in phase with the horizontal velocity but out of phase by $\pi/2$ relative to the vertical velocity. Since the net influence of magneto-acoustic waves on spectral lines lies in their phase correlations (Solanki & Roberts 1992), the asymmetry produced by horizontally propagating MAGS-waves vanishes at disc centre.

We have used a model configuration in which the upper magnetic atmosphere is cooler than the underlying quiet convection zone giving rise to two types of modes: a slow magneto-acoustic mode and (trapped) harmonic modes, the lowest of which is a magnetically modified f-mode. Whereas the former decays monotonically away from the interface and mainly influences the line wings formed low in the atmosphere, the latter may reach higher up and also induce a shift of the line core. The sign of the asymmetry seen towards the limb changes, depending on whether the waves are propagating towards (red-shifted line profiles) or away from the observer (blue-shifted line profiles). Hence, the blue- and red-shifts seen in the discward and limbward penumbra of sunspots, respectively, can be explained by MAGS-waves propagating from the outer penumbra towards the umbra. The only directly observed waves in the penumbra are the outward propagating running penumbral waves (Giovanelli 1972). Although these waves have also been modelled by surface waves (Nye & Thomas 1976b), they are quite distinct from the surface waves considered in the present paper which have wavelengths close to or below the current spatial resolution limit.

This result and the known phase relation between horizontal velocity and temperature allow further conclusions to be drawn. The horizontal phase velocity vector is parallel to the direction of propagation when the temperature is high, and anti-parallel when the temperature is low. Combining this with the sense of the net line shift implies that the spatially averaged profile obtains its largest contribution from the low-temperature regions. Consequently, the asymmetry and shift of the spatially averaged line profile is mainly due to the correlation between line strength and velocity and to a much smaller extent to the correlation between continuum intensity and velocity. Therefore, we expect that lines with different properties will also show different net shifts and asymmetries. Such differences are observed (e.g. Ichimoto 1987). One should, however, keep in mind the simplicity of our linear model. Extensions such as the consistent determination of the linear eigenmodes of a non-isothermal atmosphere, the inclusion of radiative energy exchange, or a proper non-linear calculation of surface waves may well introduce changes which affect the phase correlations and hence the line profiles significantly. Furthermore, efficient radiative energy exchange may attenuate the temperature fluctuations caused by the waves (except maybe for the harmonics; cf. Fig. 3). In addition, there is some observational evidence that the Evershed effect is limited to a fraction of penumbral filaments only (e.g., Mamadazimov 1972; Title et al. 1992). A superposition of profiles from two such components should also affect the spectral signature.

One major shortcoming of the present model is the requirement of a magnetopause very close to the $\tau_c = 1$ level throughout the penumbra. This contradicts the conclusions of Solanki & Schmidt (1993), who find that sunspot penumbrae are deep, i.e., most penumbral magnetic field lines cross the $\tau_c = 1$ level within the penumbra. This implies that the model, as proposed here, cannot be correct. Surface waves may nevertheless be responsible for the Evershed effect. There is increasing evidence that the magnetic field in sunspot penumbrae is filamentary on the scale of the white-light filaments (e.g. Beckers & Schröter 1969; Degenhardt & Wiehr 1991; Title et al. 1992; Schmidt et al. 1992). Broad-band circular polarization measurements (e.g. Illing et al. 1975; Makita & Ohki 1986) require that the field is also strongly filamented in the vertical direction (Solanki & Montavon 1993). Consequently, there exist horizontal interfaces between two magnetic components of different field strength and direction within the penumbra. Surface waves travelling along such interfaces should also produce the spectroscopic signature of the Evershed effect.

In summary, we have presented surface waves as an alternative to the classical interpretation of the Evershed effect as a steady flow. Although surface waves – within the limits of this exploratory investigation – explain a number of basic observations without suffering from the disadvantages of steady flows, we believe that only further modelling and observations will show whether they really are responsible for the Evershed effect, or if other dynamic phenomena (see e.g. Wentzel 1992) lie at its origin.

Acknowledgements. We thank B. Roberts and A. Miles for providing results ahead of publication and for clarifying discussions. We also thank M. Schüssler and T. Bogdan for commenting on the manuscript. The work of one of us (M.B.) was financially supported by the Swiss National Science Foundation under grant no. 20-31 289.91.

Appendix A: magneto-acoustic gravity waves

The linearized basic equations (Sect. 2.1) allow solutions of the form $v_{1z} = \hat{v}_{1z}(z)\exp[i(\omega t + k_x x)]$ for all of the perturbed quantities. The problem then reduces to one ordinary differential equation in one of the perturbations, e.g. $\hat{v}_{1z}$:

$$\frac{\mathrm{d}}{\mathrm{d}z}\left[\rho_0\frac{(c_S^2+v_A^2)\,(\omega^2-k_x^2c_T^2)}{k_x^2c_S^2-\omega^2}\frac{\mathrm{d}\hat{v}_{1z}}{\mathrm{d}z}\right]-\left[\rho_0\,(\omega^2-k_x^2v_A^2)+\frac{g^2\rho_0k_x^2}{k_x^2c_S^2-\omega^2}+gk_x^2\frac{\mathrm{d}}{\mathrm{d}z}\left(\frac{\rho_0c_S^2}{k_x^2c_S^2-\omega^2}\right)\right]\hat{v}_{1z}=0\,. \qquad (A1)$$

The amplitudes of all the other perturbations can be expressed in terms of $\hat{v}_{1z}$ and its first derivative:

$$\left.\begin{aligned}
\hat{v}_{1x} &= \frac{ik_x}{k_x^2c_S^2-\omega^2}\left(g\hat{v}_{1z}-c_S^2\frac{\mathrm{d}\hat{v}_{1z}}{\mathrm{d}z}\right)\,,\\
\hat{p}_1 &= \frac{i}{\omega(k_x^2c_S^2-\omega^2)}\left\{\left[k_x^2c_S^2\left(\rho_0g+\frac{\mathrm{d}p_0}{\mathrm{d}z}\right)-\omega^2\frac{\mathrm{d}p_0}{\mathrm{d}z}\right]\hat{v}_{1z}-\rho_0c_S^2\omega^2\frac{\mathrm{d}\hat{v}_{1z}}{\mathrm{d}z}\right\}\,,\\
\hat{\rho}_1 &= \frac{i}{\omega(k_x^2c_S^2-\omega^2)}\left\{\left[k_x^2\left(\rho_0g+c_S^2\frac{\mathrm{d}\rho_0}{\mathrm{d}z}\right)-\omega^2\frac{\mathrm{d}\rho_0}{\mathrm{d}z}\right]\hat{v}_{1z}-\rho_0\omega^2\frac{\mathrm{d}\hat{v}_{1z}}{\mathrm{d}z}\right\}\,,\\
\hat{T}_1 &= \frac{i}{\omega(k_x^2c_S^2-\omega^2)}\left\{\left[(\gamma-1)k_x^2g+(k_x^2c_S^2-\omega^2)\cdot\frac{1}{T_0}\frac{\mathrm{d}T_0}{\mathrm{d}z}\right]\hat{v}_{1z}-(\gamma-1)\omega^2\frac{\mathrm{d}\hat{v}_{1z}}{\mathrm{d}z}\right\}T_0\,,\\
\hat{B}_{1x} &= \frac{i}{\omega}\left[\frac{\mathrm{d}B_0}{\mathrm{d}z}\hat{v}_{1z}+B_0\frac{\mathrm{d}\hat{v}_{1z}}{\mathrm{d}z}\right]\,,\\
\hat{B}_{1z} &= -\frac{k_x}{\omega}B_0\hat{v}_{1z}\,.
\end{aligned}\right\} \qquad (A2)$$

ρ_0 is the mass density, g the gravitational acceleration, $c_S = \sqrt{\gamma p_0/\rho_0}$ the isothermal sound speed (with gas pressure p_0), $\gamma = c_p/c_V$ the adiabatic exponent, $v_A = B_0/\sqrt{4\pi\rho_0}$ the Alfvén speed (with magnetic field strength B_0), $c_T = v_Ac_S/\sqrt{v_A^2+c_S^2}$ the tube (cusp) speed, and the magnetic permeability has been set to unity.

Appendix B: surface waves in the two-layer model

Equation (A1) can be solved analytically for the two-layer model described in Sect. 2, i.e. two isothermal layers, the upper one of which is homogeneously magnetized. The constraint of a finite total energy density requires that the physically interesting solution is bounded for $|z| \to \infty$. Requiring continuity of $\hat{v}_{1z}$ at the interface $z = 0$ and choosing a convenient normalization, the solution is found to be

$$\hat{v}_{1z}(z) = \hat{v}_{1z}(0)\begin{cases}\dfrac{F(p,q;r;X_i(z))}{F(p,q;r;X_{i0})}\exp(-zk_x)\,, & z>0\\[2ex] \exp\left[z\left(\dfrac{1}{2H_e}+M_e\right)\right]\,, & z<0\end{cases} \qquad (B1)$$

where F is the hypergeometric function with parameters p, q, r, and argument $X_i(z) = X_{i0}\exp(-z/H_i)$, and $H_{i,e}$ are the respective pressure scale heights. The various quantities appearing in Eq. (B1) are given by

$$\begin{aligned}
X_{i0} &= -\frac{c_i^2\omega^2}{(\omega^2-k_x^2c_i^2)v_A^2}\,,\\
p\,,\ q &= \frac{1}{2}+k_xH_i\\
&\quad\pm\frac{1}{2}\left\{1-\left(\frac{\omega}{\omega_{ai}}\right)^2+4(H_ik_x)^2\left[1-\left(\frac{\omega_{gi}}{\omega}\right)^2\right]\right\}^{1/2}\,,\\
r &= p+q = 1+2k_xH_i\,,\\
M_e &= \frac{1}{2H_e}\sqrt{1-4A_eH_e^2}\,,\\
A_e &= \frac{1}{c_e^2\omega^2}\left[g^2k_x^2(\gamma-1)+\omega^2\left(\omega^2-k_x^2c_e^2\right)\right]\,.
\end{aligned} \qquad (B2)$$

In writing Eq. (B2) we have introduced the frequencies $\omega_{ai} = c_i/(2H_i)$ and $\omega_{gi} = c_i\sqrt{\gamma-1}/(\gamma H_i)$, which denote the acoustic cutoff and the buoyancy (Brunt-Väisälä) frequencies for the isothermal, magnetic medium (index i), respectively. Note that p and q are complex conjugates so that r is always real. The complete functional form of the other atmospheric perturbations follow from Eqs. (A2). The dispersion relation of the system arises from the pressure balance at the interface (at $z = 0$)

$$\rho_i\frac{(c_i^2+v_A^2)(\omega^2-k_x^2c_T^2)}{\omega^2-k_x^2c_i^2}\left[k_x-\frac{F'(p,q;r;X_{i0})}{F(p,q;r;X_{i0})}\right] + \frac{k_x^2g\rho_ic_i^2}{\omega^2-k_x^2c_i^2} = \frac{\rho_ec_e^2}{\omega^2-k_x^2c_e^2}\left[k_x^2g-\left(\frac{1}{2H_e}+M_e\right)\omega^2\right]\,, \qquad (B3)$$

where now $v_A = v_A(0)$, $c_T = c_T(0)$, and $F'(p,q;r;X_{i0}) = -pqX_{i0}\,F(p+1,q+1;r+1;X_{i0})/(rH_i)$. Note that Eq. (B3) requires the computation of the hypergeometric function F for arguments $X_{i0} < -1$ for modes with $\omega > k_xc_i$ ($Y > c_i/c_e$). For this it is convenient to use the linear transformation [15.3.7] of Abramowitz & Stegun (1965) and to follow Press et al. (1986) in the evaluation of the complex valued Gamma function. This procedure yields a relative accuracy in F of generally better than 10^{-9}, sufficient for our purposes. The mode structure of our model is shown in Fig. 2, the eigenmodes with $\lambda_x = 63.4$ km are plotted in Fig. 3. For more details we refer to Nye & Thomas (1976a) and Miles et al. (1992).

References

Abramowitz, M., Stegun, I.A., 1965, Handbook of mathematical functions, Dover Publications, Inc., New York

Beckers, J.M., Schröter, E.H.: 1969, SP 10, 384
Darconza, G.: 1992, Diplomarbeit, ETH Zürich
Degenhardt, D., Wiehr, E.: 1991, A&A 252, 821
Ding, M.D., Fang, C.: 1989, A&A 225, 204
Evershed, J.: 1909, MNRAS 69, 454
Giovanelli, R.G.: 1972, SP 27, 71
Gustafsson, B.: 1973, Uppsala Astron. Obs. Ann. 5, No. 6
Ichimoto, K.: 1987, PASJ 39, 329
Illing, R.M.E., Landman, D.A., Mickey, D.L.: 1975, A&A 41, 183
Jain, R., Roberts, B.: 1991, SP 133, 263
Makita, M., Ohki, Y.: 1986, Ann. Tokyo Astron. Obs. 21, 1
Maltby, P.: 1964, Astrophys. Novegica 8, 205
Maltby, P., Eriksen, G.: 1967, SP 2, 249
Mamadazimov, M.: 1972, SP 22, 129
Meyer, F., Schmidt, H.U.: 1968, Z. Angew. Math. Mech. 48, T218
Miles, A.J., Roberts, B.: 1989, SP 119, 257
Miles, A.J., Roberts, B.: 1992, SP 141, 205
Miles, A.J., Allen, H.R., Roberts, B.: 1992, SP 141, 235
Nye, A.H., Thomas, J.H.: 1976a, ApJ 204, 573
Nye, A.H., Thomas, J.H.: 1976b, ApJ 204, 582
Press, W.H., Flannery, B.P., Teukolsky, S.A., Vetterling, W.T.: 1986, Numerical Recipies, Cambridge University Press
Roberts, B.: 1981, SP 69, 27
Schmidt, W., Hofmann, A., Balthasar, H., Tarbell, T.D., Frank, Z.A.: 1992, A&A 264, L27
Schröter, E.H.: 1965, Z. Astrophys. 62, 228
Schröter, E.H., Kentischer, T., Münzer, H.: 1989, in High Spatial Resolution Solar Observations, O. von der Lühe (ed.), National Solar Obs., Sunspot, NM, p. 229
Solanki, S.K.: 1986, A&A 168, 311
Solanki, S.K.: 1987, Ph.D. Thesis, ETH Zürich
Solanki, S.K., Roberts, B.: 1992, MNRAS 256, 13
Solanki, S.K., Montavon, C.A.P.: 1993, A&A in press
Solanki, S.K., Schmidt, H.U.: 1993, A&A 267, 287
Solanki, S.K., Montavon, C.A.P., Livingston, W.: 1992, in The Magnetic and Velocity Fields of Solar Active Regions, H. Zirin (ed.), PASPC, IAU Coll. 141, in press
Solanki, S.K., Montavon, C.A.P., Livingston, W.: 1993, A&A submitted
Spruit, H.C.: 1977, Ph.D. Thesis, Univ. Utrecht
Stellmacher, G., Wiehr, E.: 1980, A&A 82, 157
Stenflo, J.O., Harvey, J.W.: 1985, SP 95, 99
Title, A.M., Topka, K.P., Tarbell, T.D., Schmidt, W., Balke, C., Scharmer, G.B.: 1992, ApJ 393, 782
Wentzel, D.G.: 1992, ApJ 388, 211

This article was processed by the author using Springer-Verlag TEX A&A macro package 1992.